

Noise-robust computational ghost imaging with pink noise speckle patternsXiaoyu Nie ^{1,2} Fan Yang ^{1,2} Xiangpei Liu,^{1,3} Xingchen Zhao,¹ Reed Nessler ¹ Tao Peng ^{1,*}
M. Suhail Zubairy ¹ and Marlan O. Scully ^{1,4,5}¹*Texas A&M University, College Station, Texas 77843, USA*²*School of Physics, Xi'an Jiaotong University, Xi'an, Shaanxi 710049, China*³*Hefei National Laboratory for Physics Science at the the Microscale and Department of Modern Physics, University of Science and Technology of China, Hefei, Anhui 230026, China*⁴*Baylor University, Waco, Texas 76706, USA*⁵*Princeton University, Princeton, New Jersey 08544, USA*

(Received 21 March 2021; revised 29 June 2021; accepted 30 June 2021; published 13 July 2021)

We propose a computational ghost imaging (CGI) scheme using customized pink noise speckle pattern illumination. By modulating the power spectrum distribution of the speckles, we generate speckle patterns with a significant positive spatial intensity fluctuation correlation. We experimentally reconstruct images using our synthesized speckle patterns in the presence of a variety of noise sources and pattern distortion and show it is robust to noise environment. The results are compared with the use of standard white noise speckle patterns. We show that our method gives much better image qualities under different types of noise than the traditional way. The proposed scheme promises potential applications in underwater, dynamic, and moving target CGI.

DOI: [10.1103/PhysRevA.104.013513](https://doi.org/10.1103/PhysRevA.104.013513)**I. INTRODUCTION**

Ghost imaging (GI), which can be realized in both quantum and classical light [1–4], is an alternative to the conventional image capture method using digital cameras. One major ameliorated system, computational ghost imaging (CGI), only employs one single-element detector to reconstruct images [5]. The predetermined speckle patterns for CGI are performed with spatial light modulators (SLM) [6], digital micromirror devices (DMD) [7], LED arrays [8], or optical phased arrays [9]. CGI also grants advantages in an expanding range of nonconventional applications such as wide spectrum imaging [7,10] and depth mapping [11,12]. Moreover, CGI can be applied to images with spatially variant and reconfigurable resolution [13–15].

By measuring the second-order correlation between the intensities of two light paths, thermal light GI can significantly eliminate disturbance from turbulence during the process of light propagation [16,17]. Underwater CGI has also been demonstrated to attenuate the disturbance from the environment noise under certain conditions [18]. To date, several studies such as differential detection [19,20], monitoring the noise [21], balanced detection [22], and microscanning techniques [23–25] have been employed with CGI to decrease the influence of system noise further and enhance the signal-to-noise ratio. However, these methods are usually limited to a particular type of noise or require a large amount of extra work to eliminate the noise influence. On the other hand, orthogonal sampling strategies [26,27], compressive sensing GI [28–30], and deep learning GI [31] have been recently

explored to obtain better image quality. These methods help shorten the signal acquisition time by reducing the total number of correlation measurements. However, these technologies rely on preknowledge of the imaging system in advance. For example, compressive sensing GI needs prior understanding of the scene, such as sparsity constraints, to guide the image reconstruction. The deep learning GI method requires us to prepare thousands of training figures to develop convolutional neural networks. Improving the image quality of CGI without knowing image information, with general noises from background light, media scattering, pattern distortion, etc., remains challenging.

By modulating the phase at the Fourier plane, speckle patterns with desired probability density functions were achieved experimentally [32]. More recently, a subdiffraction-limited resolution microscopy was demonstrated using such a scheme [33]. Different than modulating the phase front, we recently generated synthesized speckles via power spectrum distribution (PSD) modulation of the input light on the spatial frequency domain and achieved superresolving second-order correlation imaging with the obtained speckle illumination [34]. In this work, we adapt the pink noise concept to the spatial frequency domain of speckle patterns. Pink noise has been used to model electronic noise [35] and the statistical structure of natural images [36], and it is also one of the most common signals in biological systems [37]. We show a nontrivial positive correlation between a pixel and its neighbors in pink noise speckles. We then present a robust CGI scheme with the pink noise speckle patterns. The measurements are performed under several different types of noise. We also compare the results with the commonly used white noise speckle patterns.

*taopeng@tamu.edu

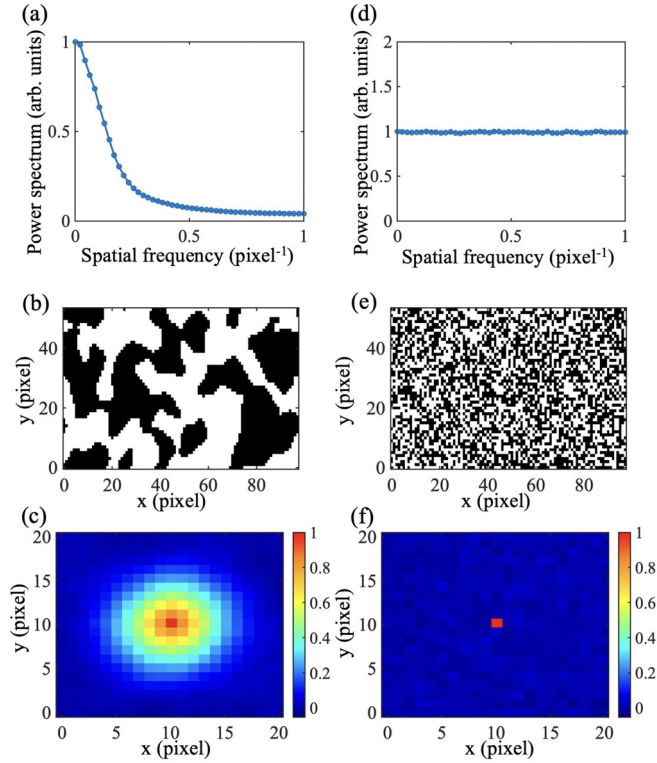


FIG. 1. (a), (b), and (c): The 1D PSD, a typical speckle pattern, and spatial intensity fluctuation correlation of customized pink noise patterns. (d), (e), and (f): The 1D PSD, a typical speckle pattern, and spatial intensity fluctuation correlation of standard white noise patterns. Compared with white noise, there is a strong positive cross-correlation between a pink noise pixel and its neighbors.

II. CHARACTERISTICS OF PINK NOISE SPECKLES

Speckles for GI are generally produced by scattering laser light off a ground glass diffuser [38] or modulating the laser light using a SLM [6]. Here we introduce colored noise speckle patterns. The PSD of the speckles is $I(\omega) \simeq C_1\delta(\omega) + C_2\omega^n$ for spatial frequency ω , where C_1 and C_2 are the coefficients of the *DC* and colored noise (*AC*) spectrum components, respectively. Since the *DC* part only contributes a constant background of the intensity, and it does not affect the intensity fluctuation correlation, we will only focus on the *AC* components hereafter. For the standard white noise speckle patterns, $n = 0$. For pink noise, we have $n = -1$, in which the PSD decreases with spatial frequency. The PSD of pink noise and white noise used in the experiment are shown in Figs. 1(a) and 1(d), respectively. A two-dimensional (2D) symmetrical conjugate random-phase matrix is assigned to the 2D power spectrum we prepared in advance. The grayscale Gaussian pink and white noise patterns are then obtained via the inverse Fourier transform. Last we convert the patterns from grayscale to binary, which can be conveniently applied on the DMD later. The generated speckle patterns are shown in Figs. 1(b) and 1(e) for pink noise and white noise. The PSD maintain their desired distributions, i.e., pink noise and white noise PSD. Next, we examine the fluctuation correlation of the speckle patterns. To simplify the calculation without loss of generality, we consider here the 1D case with positive

frequencies. The spatial intensity fluctuation correlation is defined as

$$\begin{aligned} \Gamma^{(2)}(\Delta x) &\equiv \langle I(x)I(x + \Delta x) \rangle - \langle I(x) \rangle \langle I(x + \Delta x) \rangle \\ &= \mathcal{F}^{-1}\{|C_2\omega^n|^2\}(\Delta x). \end{aligned} \quad (1)$$

For white noise speckles ($C_2 = C_w$), there is no correlation between adjacent pixels

$$\Gamma_w^{(2)}(\Delta x) = \mathcal{F}^{-1}\{|C_w|^2\}(\Delta x) \propto \delta(\Delta x). \quad (2)$$

The pixelwise spatial correlation rapidly decays to zero, as shown in Fig. 1(f).

For pink noise speckles ($C_2 = C_p$), we have the intensity fluctuation correlation as

$$\Gamma_p^{(2)}(\Delta x) = \mathcal{F}^{-1}\{|C_p\omega^{-1}|^2\}(\Delta x). \quad (3)$$

If we examine the correlation with ω_1 as the lowest frequency allowed which follows the pink noise PSD [39], and ω_2 as the upper bound positive frequency used, Eq. (3) becomes

$$\begin{aligned} \Gamma_p^{(2)}(\Delta x) &\propto \int_{\omega_1}^{\omega_2} |\omega^{-1}|^2 \cos(\omega\Delta x) d\omega \\ &= \frac{\cos(\omega_1\Delta x)}{\omega_1} - \frac{\cos(\omega_2\Delta x)}{\omega_2} \\ &\quad + [\text{Si}(\omega_1\Delta x) - \text{Si}(\omega_2\Delta x)]\Delta x, \end{aligned} \quad (4)$$

where $\text{Si}(z) \equiv \int_0^z \frac{\sin t}{t} dt$ is the sine integral. Here, we note that the sin term in the integration is omitted because under the symmetrical integration, the result for odd function should be 0. The low-frequency-dominated PSD leads to a remarkable positive cross-correlation between pixels adjacent to each other. This is in contrast to white noise patterns where there is no relation between different pixels, and the ensemble of fluctuation correlation is 0. To visualize this unique nature of pink noise, we randomly pick one pixel from pink and white noise patterns and calculate its fluctuation correlation with other pixels. We can see the striking difference in Fig. 1(c) for pink noise and Fig. 1(f) for white noise. From another perspective, the shape of the object is determined by the low frequencies in the spatial frequency domain, while high frequencies indicate detailed information and boundaries. Meanwhile, the noise has typically uniformly distributive frequencies in the spatial frequency domain. Therefore, as we will show later, low-frequency-dominated speckle patterns can retrieve the image due to the relatively high signal-to-noise ratio at the low-frequency part. In contrast, traditional white noise patterns might fail to do so due to the low signal-to-noise ratio, especially at low sampling rates with the presence of strong noises.

In the imaging system, the second-order imaging is determined by the correlation function, for white noise:

$$\langle \Delta I_b \Delta I_w(x) \rangle \propto \left\langle \int dx_0 \Gamma_w^{(2)} |T(x_0)|^2 \right\rangle \approx |T(x_0)|^2, \quad (5)$$

where I_b is the bucket detector signal and $I_w(x)$ is the intensity of the white noise speckle at pixel x . $T(x_0)$ represents the object aperture function. The cross-correlation of the light on the image plane diffracted from different pixels has nearly zero contribution according to Eq. (5).

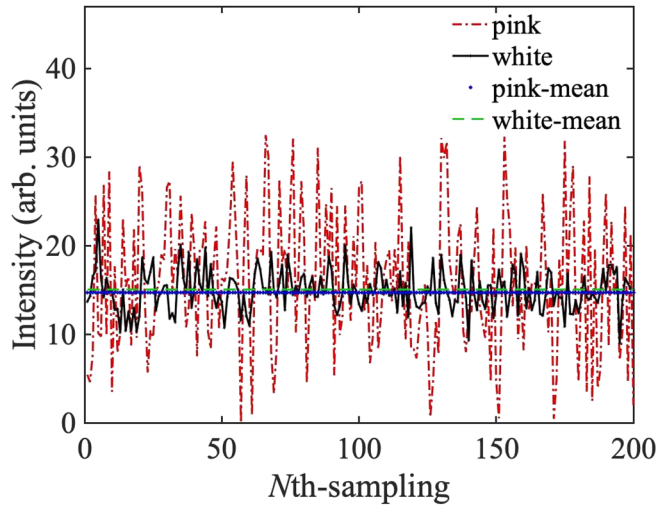


FIG. 2. Comparison of the intensity distribution for white and pink noise speckle patterns. A 10×10 pixel area was chosen on the pattern and summed up as the intensity for one-time sampling; 200 patterns are used to achieve intensity sequency that gives the intensity distribution corresponding to the sequence of patterns. The pink noise speckle (dash-dotted red line) has a much larger fluctuation as compared with the white noise speckle (solid black line), while their average intensities (“+” dotted blue line, and dashed green line) are the same.

Similarly, the second-order image measured with pink noise speckle pattern is given by

$$\langle \Delta I_b \Delta I_p(x) \rangle \propto \left\langle \int dx_0 \Gamma_p^{(2)} |T(x_0)|^2 \right\rangle. \quad (6)$$

From Eq. (6), we notice that the situation is different due to the existence of cross-correlation between light from different speckles, as shown in Eq. (4). Intuitively, we see that all the image pixels next to each other will contribute to cross-correlation with each pixel. This cross-correlation is in addition to the contribution of the autocorrelation from each pixel. The second-order signal strength is largely increased, and the noise is greatly suppressed due to the lack of correlation with other noises or the signals. To better view the advantage of using pink noise speckles vividly, we randomly pick an area of 10×10 pixels on the pattern and sum them up as the bucket detector signal. We then plot the intensity distribution from a sequence of 200 patterns for both white and pink noise speckles, as shown in Fig. 2. We see that although the average intensities are almost the same, the fluctuations are significantly different. Given that the pink noise speckles have correlation with their neighborhoods, the much more significant fluctuations associated with the pink noise pattern suggest a much stronger fluctuation correlation between a single pixel (illuminating the object area) and the bucket signal in the CGI scheme. In the next section, we will experimentally show the advantage of pink noise speckle patterns in the CGI scheme, with the presence of a variety of strong noise.

III. EXPERIMENTAL RESULTS

The experimental setup is shown in Fig. 3. A CW laser is used to illuminate the DMD where the noise patterns are

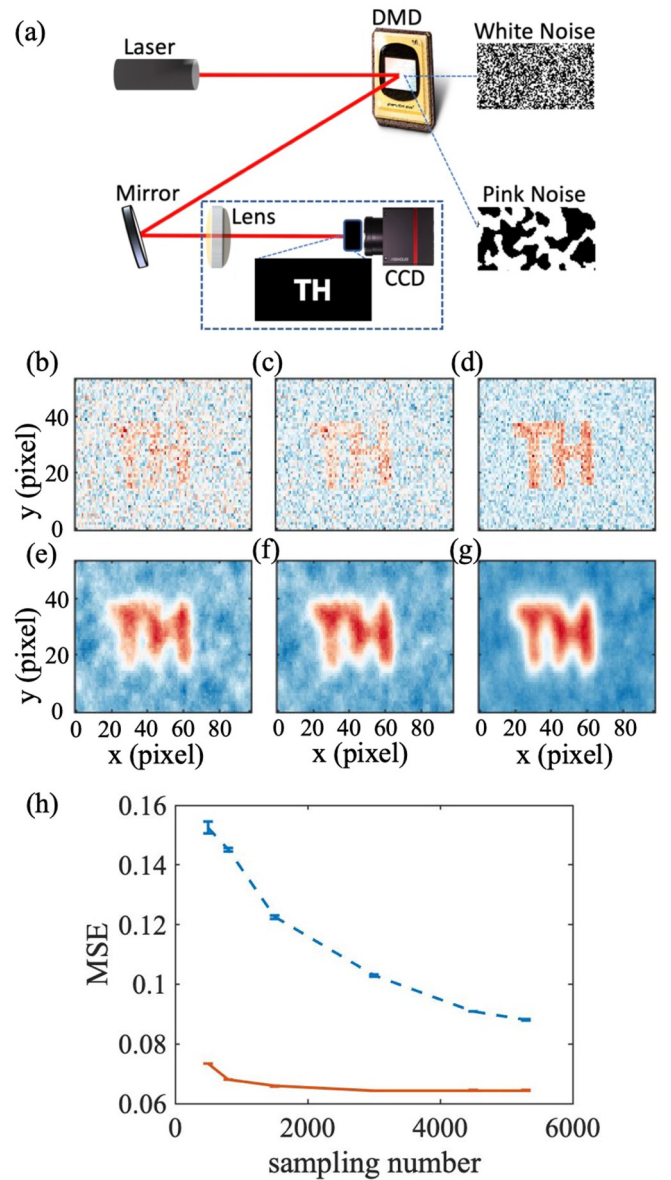


FIG. 3. (a) Schematic of the basic setup for a CGI experiment without noise. A CW laser is reflected by the DMD where the noise patterns are loaded. The reflected laser imprinted with noise patterns is imaged onto the object surface with the letters TH. A CCD put right after the object is used as a bucket detector in all the experiments in this work. The dashed frame is the part we modify by introducing a variety of noise sources. (b)–(d) CGI with white noise speckle illumination using 800, 1500, and 5292 patterns; (e)–(g) CGI with pink noise speckle illumination using 800, 1500, and 5292 patterns; (h) MSE distribution with sampling numbers of 500, 800, 1500, 3000, 4500, and 5292. The dashed blue line and solid red line correspond to the evaluation of CGI results reconstructed by white and pink noise patterns, respectively.

loaded. The pattern generated by the DMD is then imaged onto the object plane. A CCD right after the object is used as a bucket detector, i.e., only the total intensity on the CCD is used for the correlation measurement. In our experiment, the DMD contains tiny pixels (micromirrors), each measuring $16 \mu\text{m} \times 16 \mu\text{m}$. The noise pattern consists of 54×98

independent pixels (each pixel counts 4×4 DMD pixels). The object TH contains a total of about 600 independent pixels. In the following experiments, we introduce noise along the optical path between source and object, pattern distortion in addition to the optical path noise, noise on the detector, and pattern diffraction along the optical path. We perform CGI with both pink noise and white noise speckle patterns. To compare those two methods quantitatively, we introduce the mean square error (MSE) defined as

$$\text{MSE} = \frac{1}{mn} \sum_{x=1}^m \sum_{y=1}^n [CGI(x, y) - O(x, y)]^2, \quad (7)$$

where CGI is the retrieved image from CGI, O is the original object as reference, and m, n are the row and column length of the image. In our experiment, $m = 54$ and $n = 98$. We show that the pink noise speckle pattern shows a noise-robust feature for each case and gives a much lower MSE compared with the white noise. For a CGI system without introducing any noise, the results are shown in Figs. 3(b)–3(g). Overall, we note here that the image can be retrieved from both white and pink noise patterns. In the white noise case, the results have clearer edges and the quality of the image increases rapidly with the increase of sampling rate. On the other hand, pink noise results have much higher contrasts with blurring edges due to the loss of high spatial frequency components. The MSE for both cases is calculated and plotted in Fig. 3(h) as a function of the sampling numbers. We find that the MSE of pink noise patterns is very low already at low sampling number. However, for white noise results, the sub-Nyquist sampling rate does not retrieve a clear image; the quality improves continuously until full sampling number.

A. Noise between source and object

The image quality of CGI depends largely on the signal-to-noise ratio of the output intensity by the detector (the CCD in the present case). Therefore, a low noise level from both its own electronic noise and environmental noise is preferred. However, both noise sources exist in real applications. Here we use an incandescent lamp placed between DMD and the object to introduce a disturbance to the object's noise pattern illumination. The setup is shown in Fig. 4(a); 500, 800, 1500, 3000, 4500, and 5292 white and pink noise speckle patterns are used in the measurements. The typical results using 800, 1500, and 5292 sampling numbers are shown in Figs. 4(b)–4(d) under white noise sampling and Figs. 4(e)–4(g) under pink noise sampling, respectively. The MSE under various sampling numbers is present in Fig. 4(h). As compared with the no-noise case in Fig. 3, the image quality using white noise is much worse, while the image quality using pink noise does not change much. So when there is strong environmental noise along the optical path, in between the light source and the object, it is not easy to retrieve the image through a standard CGI scheme [18]. It is nevertheless shown here that using pink noise speckles can suppress the influence of such disturbance to a great extent.

B. Noise and diffuser between source and object

In reality, the environment does not simply add noise along the optical path but also introduces turbulence and distortion.

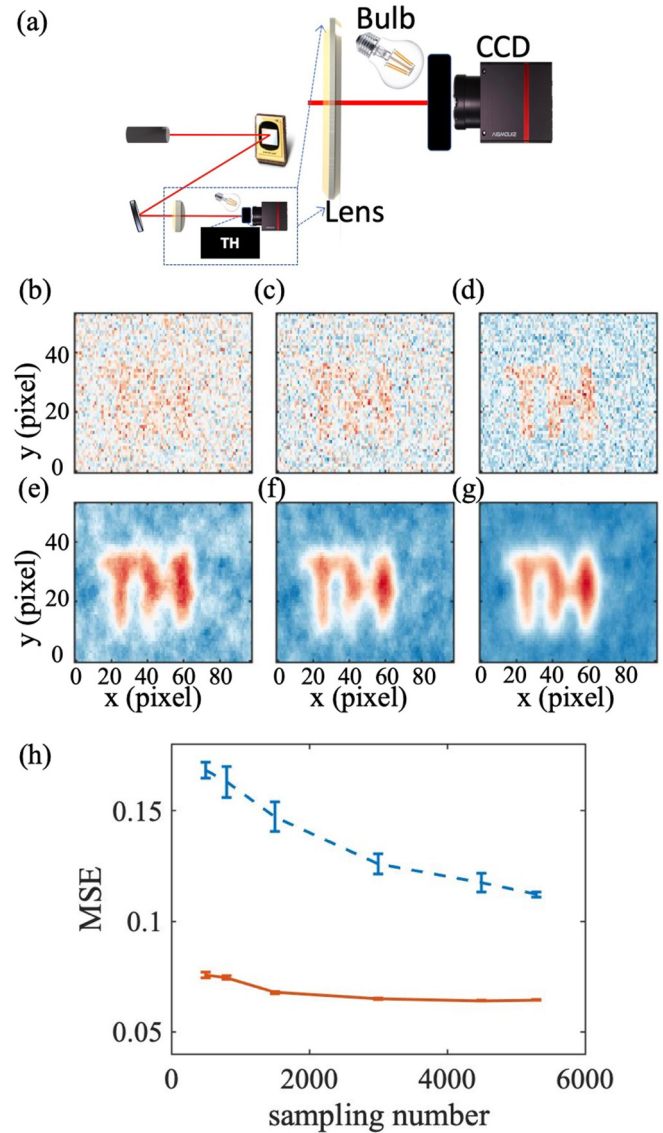


FIG. 4. (a) Schematic of the setup with environmental noise introduced by a light bulb put in front of the object; (b)–(d) CGI with white noise speckle illumination using 800, 1500, and 5292 patterns, respectively; (e)–(g) CGI with pink noise speckle illumination using 800, 1500, and 5292 patterns, respectively. CGI with white noise is blurred until distinguishable from background noise at full sampling (5292) due to the strong background noise, while the CGI with pink noise retrieves the image at low sampling rate; (h) MSE distribution with sampling number at 500, 800, 1500, 3000, 4500, and 5292. The dashed blue line and solid red line correspond to evaluation on CGI results reconstructed by white and pink noise patterns. It shows that the MSE of pink noise at 500 sampling number is already better than the white noise at full sampling number (5292).

It has been shown that distortion along the optical path will greatly affect the image quality [18]. In addition to the incandescent lamp, we add a ground glass diffuser between the lens and object to introduce diffraction and background noise simultaneously. This mimics the situation that the patterns are both smeared and buried in background noise. The schematic is shown in Fig. 5(a). The CGI results by averaging 800, 1500, and 5292 speckle patterns are shown in Figs. 5(b)–5(d) for

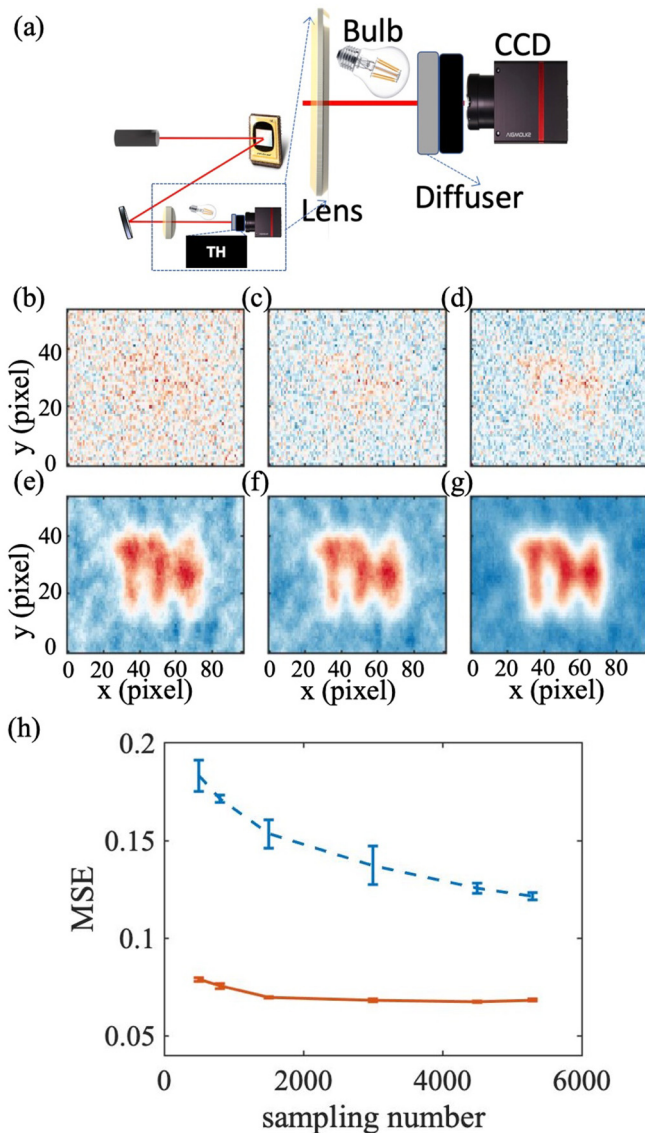


FIG. 5. (a) Schematic of the setup. A ground glass diffuser (grit size 220) is put in front of the object to diffuse the speckle patterns, and a light bulb is also put in front of the object to introduce further environment noise; (b)–(d) CGI with white noise speckle illumination using 800, 1500, and 5292 patterns; (e)–(g) CGI with pink noise speckle illumination using 800, 1500, and 5292 patterns. CGI with white noise is blurred and indistinguishable even at full sampling (5292) due to the strong background noise and diffraction, while the CGI with pink noise shows the image; (h) MSE distribution with sampling numbers of 500, 800, 1500, 3000, 4500, and 5292. The dashed blue line and solid red line correspond to the evaluation of CGI results reconstructed by white and pink noise patterns, respectively.

white noise and Figs. 5(e)–5(g) for pink noise, respectively. The white noise patterns cannot retrieve the image even at the full sampling number 5292, while pink noise patterns, on the other hand, can reconstruct the image with good quality even at the 800 sampling number. From Fig. 5(h) we see that the MSE difference between results from the 800 sampling number is around 0.1. By comparing Figs. 5(d) and 5(g) to Figs. 4(d) and 4(g), we can conclude that the distortion effect

made from ground glass has significant influence on white noise patterns because of the obvious quality decline at 5292 sampling number; nevertheless, it does not make much difference on pink noise CGI. Therefore, the introduction of the glass diffuser in the optical path decreases the image quality using white noise to a great extent, but it does not affect pink noise imaging much. This again is a demonstration of the robustness of pink noise CGI.

C. Diffraction of speckle patterns

In this part of our experiment, we put an iris right after the lens, which is used to image the speckle patterns on the object plane, as shown in Fig. 6(a). In the iris's presence, the speckles can no longer maintain their spatial distribution as loaded on the DMD. Therefore the bucket detector-recorded intensity is a mixture of desired speckles and unwanted speckles. The GI is expected to be destroyed since the one-to-one correspondence of the CGI is no longer valid. Indeed, the retrieved image from 800 white noise speckle patterns, as shown in Fig. 6(b), is almost blurred. The image has very poor quality even at the full sampling number case, as shown in Fig. 6(d). On the other hand, pink noise CGI is still able to retrieve an image of the object with 800, 1500, and 5292 patterns, as shown in Figs. 6(e)–6(g); in (h), MSE distribution with sampling numbers of 500, 800, 1500, 3000, 4500, and 5292. As expected, the MSE value of the white noise case (dashed blue line) is higher than previous measurements, but remains low for the pink noise case (solid red line).

D. Noise between object and detector

To further demonstrate the strength of pink noise CGI, we enhance the noise level by placing an incandescent lamp that produces strong light noise between the object and the CCD. Under certain circumstances, such as in biomedical applications, the signal is weak due to significant attenuation and diffusion along the optical path. In such cases, the signal at the detector could be below the detector noise level. Here we show that even in those extreme situations, our scheme can still retrieve the object image. As shown in Fig. 7(a), the lamp introduces noise distributed uniformly on the CCD plane to mimic strong noise from the bucket detector. To be more specific, the noise intensity of each pixel is around 240 units, whereas the transmitted signal is only around 7 to 8 units. The experimental results are presented in Figs. 7(b)–7(d) for white noise illumination and Figs. 7(e)–7(g) for pink noise illumination. Here, due to the extreme background noise at the detector, 5292 patterns still cannot retrieve the image in the white noise case as shown in Fig. 7(d). The MSE in Fig. 7(h) of white noise does not decrease when we increase the sampling number. However, the pink noise in CGI can retrieve the image of the object. The TH can be clearly seen by using 5292 pink noise patterns. From MSE in Fig. 7(h), we see that the pink noise can fully retrieve the image under 3500 sampling number, after which MSE goes smoothly. In this situation, the pink noise CGI can reconstruct images in some typical situations that white noise CGI cannot retrieve the image at all.

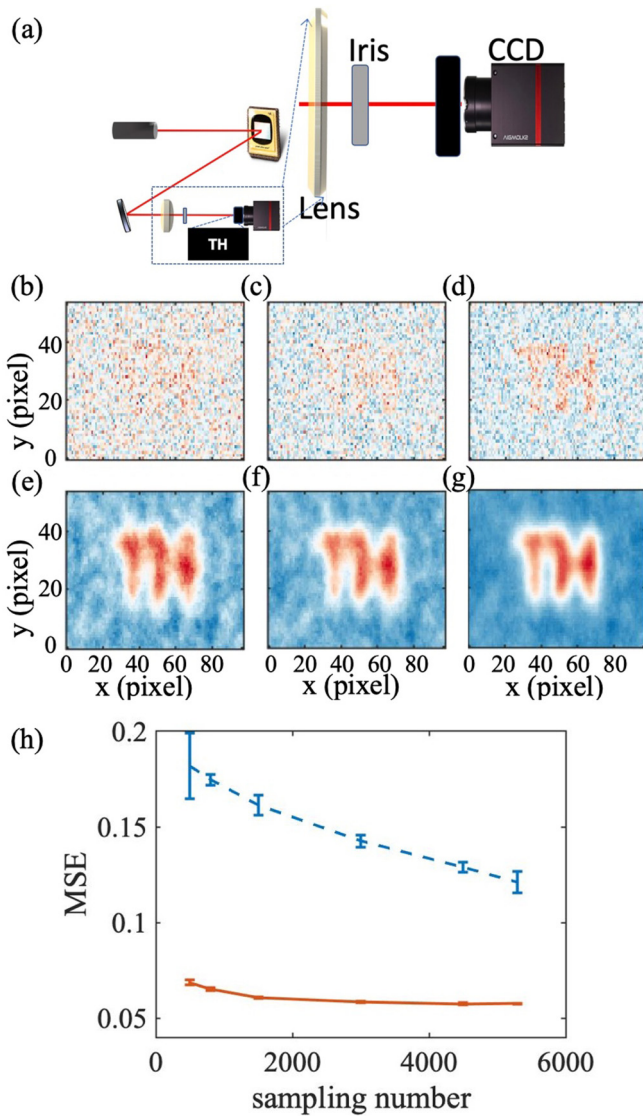


FIG. 6. (a) Schematic of the setup with an iris inserted right after the lens. The diameter of the iris is $1000 \mu\text{m}$. The speckle patterns are diffracted due to the iris; (b)–(d) CGI with white noise speckle illumination using 800, 1500, and 5292 patterns; (c)–(f) CGI with pink noise speckle illumination using 800, 1500, and 5292 patterns. CGI with white noise is blurred and indistinguishable at 800 and 1500 sampling number and has low contrast to background at 5292. However, the CGI with pink noise retrieves clear images; (h) MSE distribution with sampling numbers of 500, 800, 1500, 3000, 4500, and 5292. The dashed blue line and solid red line correspond to the evaluation of CGI results reconstructed by white and pink noise patterns, respectively.

IV. SUMMARY

We have developed a method to create the pink noise speckle pattern and applied it to the CGI system. The modulation on the spatial frequency domain enables us to create speckle patterns that have strong positive fluctuation correlation between pixels. This feature makes it robust to noisy environment in the CGI system. The noise-robust feature of the pink noise CGI is experimentally demonstrated. We examined and compared the MSE of images retrieved by pink noise

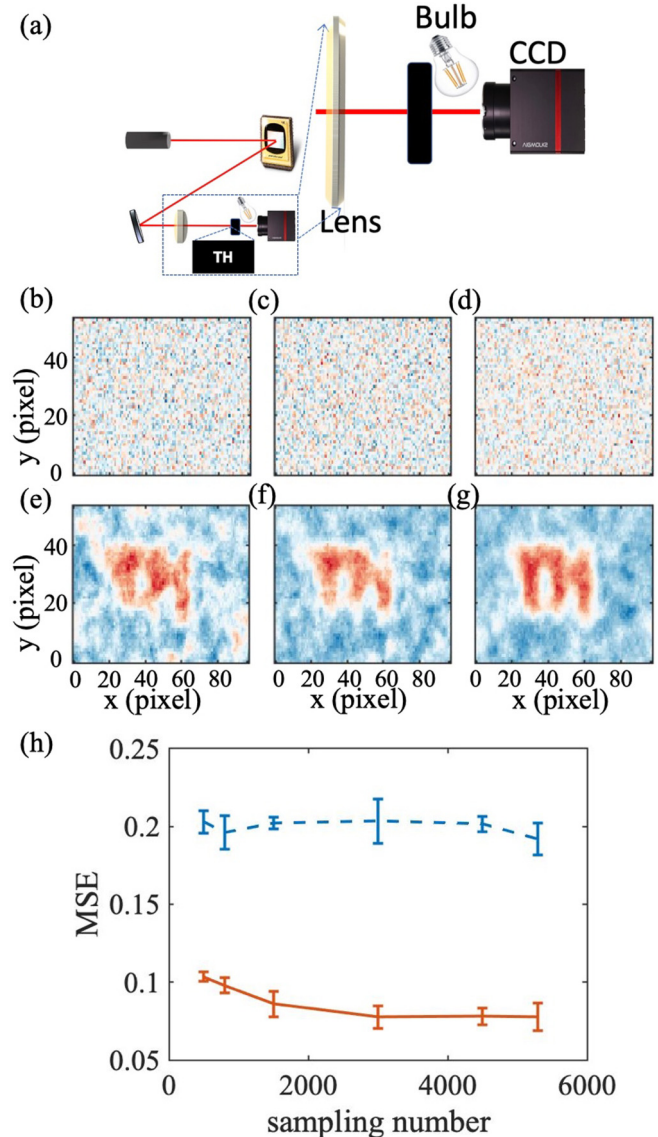


FIG. 7. (a) Schematic of the setup with environmental noise introduced by a light bulb put in front of the detector; (b)–(d) CGI with white noise speckle illumination using 800, 1500, and 5292 patterns; (c)–(f) CGI with pink noise speckle illumination using 800, 1500, and 5292 patterns. CGI with white noise is drastically blurred and totally indistinguishable even at full sampling (5292) due to the extremely strong background which even close to over exposure, while the CGI with pink noise still can retrieve the image; (h) MSE distribution with sampling numbers of 500, 800, 1500, 3000, 4500, and 5292. The dashed blue line and solid red line correspond to the evaluation of CGI results reconstructed by white and pink noise patterns, respectively.

speckle patterns and standard white noise patterns. Four types of noisy environments are introduced to mimic the random noise and pattern distortion along the optical path and the shallow signal to noise ratio at the bucket detector. We have shown that the resulting MSE of pink noise CGI is always much better than that of white noise CGI in the presence of different types of noise. This work is of great significance

for the practical application of CGI due to its robustness via substantially strong low frequency.

Pink noise pattern is one typical pattern that owns significant low frequency. Further optimization work can be done by modulating other types of PSF to adjust the intensity fluctuation correlation function. Also, further amelioration is to use the orthonormalization method to enhance the resolution while still keeping current advantages. Combining compressive sensing or deep learning methods with pink noise patterns can reach extremely low sampling rates while maintaining the image quality in CGI.

ACKNOWLEDGMENTS

X.N. and F.Y. thank A. Svidzinsky for his kind help during their visit to IQSE, Texas A&M University. We gratefully acknowledge the support of the Air Force Office of Scientific Research (Award No. FA9550-20-1-0366 DEF), the Office of Naval Research (Award No. N00014-20-1-2184), the Robert A. Welch Foundation (Grant No. A-1261), the National Science Foundation (Grant No. PHY-2013771), and the Qatar National Research Fund (Project NPRP 13S-0205-200258).

X.N. and F.Y. contributed equally to this work.

-
- [1] T. B. Pittman, Y. H. Shih, D. V. Strekalov, and A. V. Sergienko, *Phys. Rev. A* **52**, R3429(R) (1995).
- [2] R. S. Bennink, S. J. Bentley, and R. W. Boyd, *Phys. Rev. Lett.* **89**, 113601 (2002).
- [3] A. Valencia, G. Scarcelli, M. D'Angelo, and Y. Shih, *Phys. Rev. Lett.* **94**, 063601 (2005).
- [4] X.-H. Chen, Q. Liu, K.-H. Luo, and L.-A. Wu, *Opt. Lett.* **34**, 695 (2009).
- [5] J. H. Shapiro, *Phys. Rev. A* **78**, 061802(R) (2008).
- [6] Y. Bromberg, O. Katz, and Y. Silberberg, *Phys. Rev. A* **79**, 053840 (2009).
- [7] N. Radwell, K. J. Mitchell, G. M. Gibson, M. P. Edgar, R. Bowman, and M. J. Padgett, *Optica* **1**, 285 (2014).
- [8] Z.-H. Xu, W. Chen, J. Penuelas, M. Padgett, and M.-J. Sun, *Opt. Express* **26**, 2427 (2018).
- [9] L.-J. Li, W. Chen, X.-Y. Zhao, and M.-J. Sun, *IEEE Photon. J.* **11**, 1 (2019).
- [10] M. P. Edgar, G. M. Gibson, R. W. Bowman, B. Sun, N. Radwell, K. J. Mitchell, S. S. Welsh, and M. J. Padgett, *Sci. Rep.* **5**, 10669 (2015).
- [11] G. A. Howland, D. J. Lum, M. R. Ware, and J. C. Howell, *Opt. Express* **21**, 23822 (2013).
- [12] M.-J. Sun, M. P. Edgar, G. M. Gibson, B. Sun, N. Radwell, R. Lamb, and M. J. Padgett, *Nat. Commun.* **7**, 12010 (2016).
- [13] D. B. Phillips, M.-J. Sun, J. M. Taylor, M. P. Edgar, S. M. Barnett, G. M. Gibson, and M. J. Padgett, *Sci. Adv.* **3**, e1601782 (2017).
- [14] M.-J. Sun, X.-Y. Zhao, and L.-J. Li, *Opt. Lett.* **43**, 4049 (2018).
- [15] M. Aßmann and M. Bayer, *Sci. Rep.* **3**, 1545 (2013).
- [16] R. E. Meyers, K. S. Deacon, and Y. Shih, *Appl. Phys. Lett.* **98**, 111115 (2011).
- [17] Y. Shih, H. Chen, and T. Peng, Turbulence-free camera system and related method of image enhancement, US Patent No. 9,444,978 (2016).
- [18] M. Le, G. Wang, H. Zheng, J. Liu, Y. Zhou, and Z. Xu, *Opt. Express* **25**, 22859 (2017).
- [19] F. Ferri, D. Magatti, L. A. Lugiato, and A. Gatti, *Phys. Rev. Lett.* **104**, 253603 (2010).
- [20] B. Sun, M. Edgar, R. Bowman, L. Vittert, S. Welsh, A. Bowman, and M. Padgett, *Imaging and Applied Optics*, OSA Technical Digest (Optical Society of America, 2013), p. CTu1C.4.
- [21] Z. Yang, Y. Sun, S. Qu, Y. Yu, R. Yan, A.-X. Zhang, and L.-A. Wu, *Appl. Opt.* **57**, 6097 (2018).
- [22] F. Soldevila, P. Clemente, E. Tajahuerce, N. Uribe-Patarroyo, P. Andrés, and J. Lancis, *Sci. Rep.* **6**, 29181 (2016).
- [23] Y. Zhao, Q. Chen, X. Sui, and H. Gao, *IEEE Photon. J.* **9**, 7802111 (2017).
- [24] M.-J. Sun, M. P. Edgar, D. B. Phillips, G. M. Gibson, and M. J. Padgett, *Opt. Express* **24**, 10476 (2016).
- [25] M.-J. Sun, H.-Y. Wang, and J.-Y. Huang, *Sci. Rep.* **9**, 4105 (2019).
- [26] B. Luo, P. Yin, L. Yin, G. Wu, and H. Guo, *Opt. Express* **26**, 23093 (2018).
- [27] Z. Zhang, X. Wang, G. Zheng, and J. Zhong, *Opt. Express* **25**, 19619 (2017).
- [28] M.-J. Sun, L.-T. Meng, M. P. Edgar, M. J. Padgett, and N. Radwell, *Sci. Rep.* **7**, 3464 (2017).
- [29] V. Katkovnik and J. Astola, *JOSA A* **29**, 1556 (2012).
- [30] Z. Sheng-Mei and Z. Peng, *Chin. Phys. B* **23**, 054203 (2014).
- [31] M. Lyu, W. Wang, H. Wang, H. Wang, G. Li, N. Chen, and G. Situ, *Sci. Rep.* **7**, 17865 (2017).
- [32] N. Bender, H. Yılmaz, Y. Bromberg, and H. Cao, *Optica* **5**, 595 (2018).
- [33] N. Bender, M. Sun, H. Yılmaz, J. Bewersdorf, and H. Cao, *Optica* **8**, 122 (2021).
- [34] Z. Li, X. Nie, F. Yang, X. Liu, D. Liu, X. Dong, X. Zhao, T. Peng, M. S. Zubairy, and M. O. Scully, *Opt. Express* **29**, 19621 (2021).
- [35] P. Dutta and P. Horn, *Rev. Mod. Phys.* **53**, 497 (1981).
- [36] D. J. Field, *JOSA A* **4**, 2379 (1987).
- [37] P. Szendro, G. Vincze, and A. Szasz, *Eur. Biophys. J.* **30**, 227 (2001).
- [38] W. Martienssen and E. Spiller, *Am. J. Phys.* **32**, 919 (1964).
- [39] M. S. Keshner, *Proc. IEEE* **70**, 212 (1982).